Composite Structures 337 (2024) 118086

Contents lists available at ScienceDirect

Composite Structures

journal homepage: www.elsevier.com/locate/compstruct

Introducing a novel piezoelectric-based tunable design for mode-localized mass micro-sensors

Hossein Ali Alam-Hakkakan [a], Amir Reza Askari [b,c,*], Masoud Tahani [a,*]

[a] Department of Mechanical Engineering, Ferdowsi University of Mashhad, Mashhad, Iran
[b] Department of Mechanical Engineering, Hakim Sabzevari University, Sabzevar, Iran
[c] Department of Engineering and Technology, The University of Huddersfield, Huddersfield HD1 3DH, UK

ARTICLE INFO

Keywords:
Mode-localization phenomenon
Electrostatically coupled micro-beams
Piezoelectric excitation
High-order modes
Harmonic balance method

ABSTRACT

This investigation focuses on developing a new sensitivity-improving approach for high-order mode-localized mass micro-sensors by utilizing the capabilities of piezoelectric materials. To this end, an electrostatically coupled micro-beam as the building block of MEMS mass sensors is considered. The present design includes the incorporation of a patterned arrangement of piezoelectric thin films placed on the lower electrode of the system. The nonlinear reduced equations of motion for the introduced tunable system are derived by employing the Hamilton principle in conjunction with the Euler-Bernoulli beam theory and the Ritz discretization procedure. These equations are subsequently solved using the harmonic balance method. The present findings are validated by those available in the literature for the case of static excitation. In addition, the eigenvalue loci of the proposed system have been compared and verified by those obtained through three-dimensional finite element simulations carried out in COMSOL Multiphysics commercial software. Taking the shift of the amplitude ratio as the measure demonstrating the sensitivity of the proposed design, it is observed that incorporating piezoelectric excitation can significantly enhance the efficiency of these systems more than two times in comparison to conventional mode-localized mass micro-sensors without piezoelectric layers.

1. Introduction

Microelectromechanical systems (MEMS) are mainly operated as sensors or actuators [1]. These devices, which are used in different engineering fields, are fabricated at micro and nano scales [2]. Mass micro-sensors represent an important sub-category for MEMS devices [3]. These sensors are often manufactured as single-degree-of-freedom (sDoF) resonators [4]. The sensitivity concept associated with the resonant mass micro-sensors is defined as the shift in the resonance frequency of the device that occurred before and after the attachment of a small particle [5]. Although sDoF mass sensors are frequently used in various practical applications, they do not enjoy high sensitivity; because adding a small mass to an sDoF resonator cannot significantly change its resonance frequency [6]. Thus, multi-degree-of-freedom (mDoF) coupled resonators have been introduced as a new design for mass micro-sensors to improve their sensitivity in the past decade [7].

A new generation of high-sensitive coupled mass sensors has been developed based on employing the mode-localization phenomenon [8], first suggested by Spletzer et al. [9]. Although they did not optimize their proposed system, it represented considerably higher sensitivity compared to traditional frequency shift-based sensors. It is noteworthy that the mode-localization phenomenon refers to the concentration of vibrational energy in a small geometric region instead of the whole structure [10]. According to the mode-localization phenomenon, the presence of small irregularities in periodic structures under conditions of weak internal coupling can cause the propagation of vibration to be inhibited, and so the vibration modes are localized [11].

The mode-localized mass micro-sensors generally consist of two or more weakly coupled similar micro-resonators whose resonance zones are very close to each other. When a small particle is attached to one of the micro-resonators, the resonance frequency of that resonator undergoes a slight change. This results in a drastic change in the vibration amplitudes of the micro-resonators. That is, the vibration amplitude of the resonator on which the added mass is attached, is drastically decreased and that of the other one is dramatically increased. This change in the vibrational pattern of the resonator amplitudes, which is interpreted as the vibrational mode localization around the resonator

* Corresponding authors at: Department of Mechanical Engineering, Hakim Sabzevari University, Sabzevar, Iran (Amir R. Askari). Department of Mechanical Engineering, Ferdowsi University of Mashhad, Mashhad, Iran (M. Tahani).

E-mail addresses: ar.askari@hsu.ac.ir, a.askari@hud.ac.uk (A. Reza Askari), mtahani@um.ac.ir (M. Tahani).

https://doi.org/10.1016/j.compstruct.2024.118086
Received 15 November 2023; Received in revised form 27 January 2024; Accepted 27 March 2024
Available online 29 March 2024
0263-8223/© 2024 Elsevier Ltd. All rights reserved.

Nomenclature

b	Width of the micro-beams
c	Linear viscous damping
E_p	Young's modulus of the piezoelectric layers
E_s	Young's modulus of the micro-beams' substrate
F_c	Electrostatic attraction between the upper and lower micro-beams
F_{ele}	Electrical attraction between the lower micro-beam and the fixed electrode underneath it
g_c	Initial gap between the upper and lower micro-beams
g_a	Initial gap between the lower micro-beam and the fixed electrode underneath it
h_1	Thickness of the upper micro-beam's substrate
h_2	Thickness of the lower micro-beam's substrate
h_p	Thickness of the piezoelectric layers
$H(x)$	Unit step function
K_i	Kinetic energy of the ith micro-beam ($i = 1,2$)
L	Length of the micro-beams
L_p	Length of the piezoelectric layers
L_e	Length of the fixed substrates
M_i	Moment resultant of the ith micro-beam ($i = 1,2$)
m_p	Mass of the small particle attached on the upper micro-beam
N_i	Force resultant of the ith micro-beam ($i = 1,2$)
$q_{s1,i}$	Static counterpart of the ith ($i = 1, 2, 3, \ldots$) generalized coordinate of the upper micro-beam in the Ritz procedure
$q_{s2,i}$	Static counterpart of the ith ($i = 1, 2, 3, \ldots$) generalized coordinate of the lower micro-beam in the Ritz procedure
$q_{d1,j}(t)$	Dynamic counterpart of the jth ($j = 1, 2, 3, \ldots$) generalized coordinate of the upper micro-beam in the Ritz procedure
$q_{d2,j}(t)$	Dynamic counterpart of the jth ($j = 1, 2, 3, \ldots$) generalized coordinates of the lower micro-beam in the Ritz procedure
S_j^a	Sensitivity associated with the jth ($j = 1,2$) resonance mode
t	Time
U_i	Strain energy expression of the ith micro-beam ($i = 1,2$)
u_i	Displacements of a point located on the mid-plane of the ith micro-beam ($i = 1,2$) in the x direction
u_1	Displacement component of an arbitrary point on the micro-beam cross section along the x-direction
u_2	Displacement component of an arbitrary point on the micro-beam cross section along the y-direction
u_3	Displacement component of an arbitrary point on the micro-beam cross section along the z-direction
V_i	Volume of the ith micro-beam ($i = 1,2$)
V_{p1}	Piezoelectric voltage applied across the upper piezoelectric layers
V_{p2}	Piezoelectric voltage applied across the lower piezoelectric layers
V_{ac}	AC voltage
V_c	Coupling voltage
V_{dc}	DC voltage
W_{ext}^i	Work done by the external forces on the ith micro-beam ($i = 1,2$)
W_D	Work done by damping force
W_c	Work done by electrostatic attraction between the upper and lower micro-beams
W_{ele}	Work done by electrical attraction between the lower micro-beam and the fixed electrode underneath it
$W_{1,j}^0$	Amplitude of the upper micro-beam associated with the jth ($j = 1, 2$) resonance mode at the balanced state
$W_{2,j}^0$	Amplitude of the lower micro-beam associated with the jth ($j = 1, 2$) resonance mode at the balanced state
$W_{1,j}$	Amplitude of the upper micro-beam associated with the jth ($j = 1, 2$) resonance mode after adding small mass
$W_{2,j}$	Amplitude of the lower micro-beam associated with the jth ($j = 1, 2$) resonance mode after adding small mass
$w_1(x,t)$	Deflection of the upper micro-beam
$w_2(x,t)$	Deflection of the lower micro-beam
w_i	Displacement of a point located on the mid-plane of the ith micro-beam ($i = 1,2$) in the z-direction
x_0	Position of the small mass on the upper micro-beam
x	x-coordinate along the length of the micro-beam
y	y-coordinates along the width of the micro-beam
z	z-coordinates along the thickness of the micro-beam
$\beta_i(x)$	i^{th} ($i = 1, 2, 3, \ldots$) normalized eigenvalue of a beam with clamped boundary condition
δ	Variational operator
δ_{i2}	$i2$ ($i = 1, 2$) component of the Kronecker delta
$\delta(x-x_0)$	Dirac function
ε	Dielectric constant of the vacuum
ε_x	Axial strain in the x direction
e_{31}	Piezoelectric constant
ρ_p	Density of the piezoelectric layer
ρ_s	Density of the micro-beams' substrate
σ_x	Normal stress in the x direction
$\varphi_i(x)$	i^{th} (i = 1, 2, 3, …) linear un-damped mode-shape of a clamped beam
Ω	Excitation frequency
Ω_i	i^{th} (i = 1, 2) natural frequency of the system

without the mass-disturbance, is the sensing principle utilized in mode-localized mass micro-sensors [12]. This phenomenon is the main operation principle utilized in mode-localized resonant mass micro-sensors [13].

Given the mode-localization-based sensing principle discussed above, it is evident that introducing disorder (e.g., attaching a small particle to one of the resonators) unbalances the system, leading to the occurrence of the mode-localization phenomenon. For a more detailed investigation of this phenomenon, consider a weakly coupled 2-DoF system in its balanced state, where a veering phenomenon [14] can be observed in the loci of eigenvalues graph (i.e., a graph depicting the variation of the system eigenvalues versus the disorder parameter [15]). In this manner, applying a disorder changes the position of the system's natural frequencies so that the one corresponding to the resonator with the added mass takes place far away from the veering zone where the excitation frequency also exists. Doing so, it is apparent that the vibration mode will strongly be localized around the other resonator on which the disorder is not applied [16].

In the recent decade, mode-localization-based sensing technology has experienced significant growth with the introduction of tunable MEMS devices. Thironkatanathan et al. [17] initially introduced this new generation of tunable mode-localized mass micro-sensors by utilizing electrical actuation to establish weak coupling between the resonators. In the sequence of this work, Zhao et al. [18] proposed a 3-DoF weakly coupled system instead of the previously introduced 2-DoF device and showed that increasing the degrees of freedom enhances the sensitivity of the sensor. Rabenimanana et al. [19] developed a mode-localized mass micro-sensor consisting of two mechanically coupled micro-cantilevers with different lengths. They proposed the employment of electrostatic actuation as a reliable procedure to overcome

manufacturing defects and balance an initially unbalanced system. Pandit et al. [20] explored the possibility of employing coupled nonlinear resonators as a mode-localized mass sensor. They observed that nonlinear systems exhibit higher efficiency compared to systems operating in the linear regime. Lyu et al. [21] analyzed nonlinear 2-DoF coupled micro-beams with variable length ratios whose balance state was adjusted by the electrostatic attraction between the two electrodes. They verified their findings by those observed experimentally and showed that reducing the length ratio of the beams or decreasing the coupling between the two electrodes can improve the sensitivity.

Recently, the influence of exciting high-order modes on increasing the efficiency of mass micro-sensors has been explored by many researchers. This technique, which was first introduced by Lochon et al. [22] for sDoF mass sensors, provides the possibility of improving the sensitivity of the device without making any structural modifications. In the sequence of this work, Lyu et al. [23] analyzed a 2-DoF mass micro-sensor whose third eigenmodes are weakly coupled with each other. Doing so, they showed that the sensitivity of the device is improved up to five times. In addition, Lyu et al. [23] indicated that the sensitivity of the device can also be doubled again if the electrical excitation is applied via distributed electrodes whose layouts are more compatible with the configuration of those modes. Following this study, Zhao et al. [24] investigated the influence of coupling between dissimilar eigenmodes on the sensitivity of these systems. They discovered that if a symmetric eigenmode of one micro-beam is being coupled with an asymmetric eigenmode of the other one, the sensitivity of the sensor can drastically be improved up to 20 times greater than that corresponds to a system whose first eigenmodes are coupled to each other.

As can be seen from the literature reviewed above, the influences of electrical actuation and high-order mode excitation on the efficiency of mode-localized mass micro-sensors have been investigated in several research studies. Traditional mass MEMS sensors face limited tunability due to the fact that the electrical actuation that is used to adjust the system's balance state can only decrease the stiffness of the structure. Therefore, the idea of incorporating thin film piezoelectric materials into these conventional sensors arises, as they possess the capability to both decrease and increase the stiffness of a structure. This characteristic offers enhanced adjustability and tunability to the sensors. Hence, since the effect of piezoelectric excitation on the efficiency of mode-localized mass micro-sensors remains largely unexplored so far, the present work aims to introduce a piezoelectric-based design for mode-localized mass micro-sensors. The goal is to investigate the combined effects of the piezoelectric and electrostatic actuation on the sensitivity of such devices when their high-order eigenmodes are being excited. It is to be noted that the proposed design can present more degrees of freedom for adjusting the stiffness of the system in comparison to the traditional mode-localized mass sensors and enjoy much more sensitivity up to two times, as will be shown later.

The present paper is organized so that the details of mathematical modeling are provided in section 2. In this section, the reduced equations governing the motion of two electrically actuated coupled micro-beams are derived by adopting the Hamilton principle in conjunction with the Euler-Bernoulli beam theory and the Ritz discretization procedure. Section 3 investigates the static, free vibration, and dynamic behaviors of the present system by providing some numerical examples. This section firstly validates the present model predictions by comparing the present findings for the case of static excitation with those available in the literature. Some other comparisons are also made in this section between the present eigenvalue loci and those obtained by 3-D finite element (FE) simulations performed in COMSOL Multiphysics commercial software [25]. After a detailed parametric study, the rest of section 3 is allocated to the dynamic analysis of the present system by using the harmonic balance method. Furthermore, this section studies the combined influences of the piezoelectric and electrical actuation on the sensitivity of the proposed device. The findings indicate that incorporating piezoelectric excitation can provide a much more tunable design with higher degrees of freedom, resulting in a significant efficiency improvement more than two times compared to the designs reported by others. The main conclusions that can be drawn from the present study are summarized in section 4.

2. Mathematical modeling

Fig. 1 shows a schematic view of two clamped micro-beams that are electrically coupled to each other by applying a coupling voltage V_c. The coupling voltage adjusts the electrical attraction between the upper and lower micro-beams. The upper micro-beam (i.e., micro-beam 1) is made of a homogeneous material. Furthermore, the lower micro-beam (i.e., micro-beam 2) is made of a homogeneous substrate with a pattern of piezoelectric thin films attached to it. According to Fig. 1, x, y, and z are the coordinates along the length (L), width (b), and thickness (h_1) of the upper micro-beam, respectively. Also, g_c is the initial gap between the two micro-beams. In addition, g_a indicates the initial gap between the lower micro-beam and distributed fixed substrate electrodes. It is assumed that the upper and lower micro-beams have different thicknesses (i.e., $h_1 \neq h_2$) while other geometric properties are considered to be the same. The voltages applied across the upper and lower piezoelectric layers are indicated by V_{p1} and V_{p2}, respectively. Moreover, h_p and L_p are the thicknesses and the lengths of the piezoelectric layers, respectively. Furthermore, x_0 denotes the position of the small particle on the upper micro-beam.

According to the Euler-Bernoulli beam's hypothesis, the displacement field associated with an arbitrary point on the micro-beam cross-section can be expressed as [26]:

$$u_1 = u(x,t) - z\frac{\partial w(x,t)}{\partial x}, \quad u_2 = 0\ , \quad u_3 = w(x,t), \tag{1}$$

where u and W denote the displacements of an arbitrary point located on the mid-plane of the micro-beam in the x and z directions, respectively. Employing the von Kármán strain–displacement relation, the strain components associated with the displacement field presented in Eq. (1), can be written as follows [26]:

$$\varepsilon_x = \frac{\partial u}{\partial x} + \frac{1}{2}\left(\frac{\partial w}{\partial x}\right)^2 - z\frac{\partial^2 w}{\partial x^2}\ , \quad \varepsilon_y = \varepsilon_z = \varepsilon_{xy} = \varepsilon_{xz} = \varepsilon_{yz} = 0. \tag{2}$$

In view of the von Kármán strain–displacement introduced in Eq. (2), the expression for the variation of the strain energy associated with the

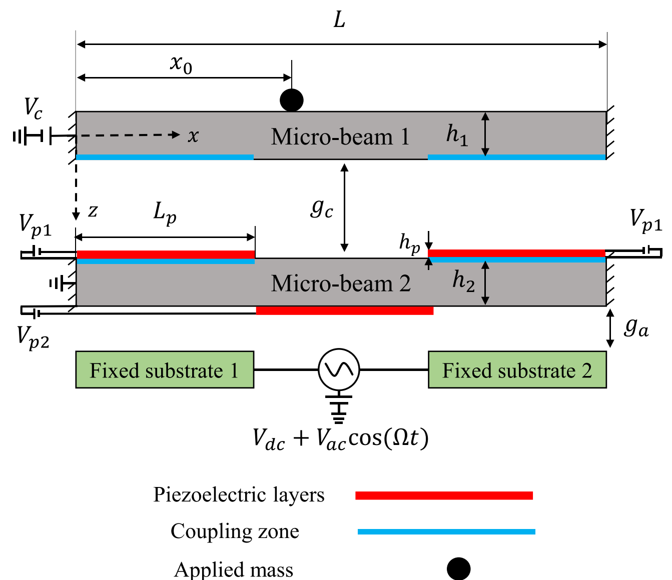

Fig. 1. Schematic view of the proposed piezoelectric-based mode-localized mass micro-sensor.

i^{th} micro-beam (i = 1, 2) is given by [27]:

$$\delta U_i = \int_{V_i} \sigma_x \, \delta \varepsilon_x dV_i = b \int_0^L \left(N_i \, \delta u_i^{'} + N_i \, w_i^{'} \, \delta w_i^{'} - M_i \, \delta w_i^{''} \right) \, dx \, , \tag{3}$$

where the prime sign denotes differentiation with respect to variable x. Furthermore, N_i and M_i are the force and moment resultants associated with the ith micro-beam (i = 1, 2), which are defined as [27]:

$$(N_i, M_i) = \int \sigma_x(1, z) dz, \tag{4}$$

Bearing in mind that the lower micro-beam (i.e., micro-beam 2) is made of three different layers, the corresponding stress–strain relations can be expressed as:

$$\sigma_x = \begin{cases} (E_p \varepsilon_x + e_{31} V_{p1}/h_p) H_1(x) & -(h_p + h_2/2) \le z \le -h_2/2 \\ E_s \varepsilon_x & -h_2/2 \le z \le h_2/2 \\ (E_p \varepsilon_x + e_{31} V_{p2}/h_p) H_2(x) & h_2/2 \le z \le (h_2/2 + h_p) \end{cases} , \tag{5}$$

where E_s denotes Young's modulus of the substrates and E_p, h_p, and e_{31} are Young's modulus, thickness, and piezoelectric constant of the piezoelectric layers. Furthermore, $H_1(x)$ and $H_2(x)$ represent the unit step functions associated with the upper and lower piezoelectric layers attached to both sides of the lower substrate which are given by:

$$H_1(x) = H(L_p - x) + H(x - (L - L_p)), \tag{6a}$$

$$H_2(x) = H\left(x - \frac{(L - L_p)}{2}\right) + H\left(x - \frac{(L + L_p)}{2}\right). \tag{6b}$$

The electrostatic excitation between the two micro-beams (F_c^i) and the electrical actuation applied on the lower micro-beam (F_{ele}), neglecting the fringing field effect, can be expressed as [28]:

$$F_c^i = \frac{\varepsilon b V_c^2 (-1)^{i+1}}{2(g_c - w_1 + w_2)^2} H_e(x), \tag{7}$$

$$F_{ele} = \frac{\varepsilon b (V_{dc} + V_{ac} \cos(\Omega t))^2}{2(g_a - w_2)^2} H_e(x),$$

where $w_1(x, t)$ and $w_2(x, t)$ are the deflections of the upper and lower micro-beams and $\varepsilon = 8.854 \times 10^{-12}$ (Fm^{-1}) is the dielectric constant of the vacuum [29]. Also, V_{dc} and V_{ac} represent the amplitude of the DC and AC voltages. Moreover, Ω and $H_e(x)$ are the excitation frequency and unit step function associated with the electrical excitation applied by distributed electrodes, which can be expressed as:

$$H_e(x) = H(L_e - x) + H(x - (L - L_e)), \tag{8}$$

where L_e is the length of each distributed electrode.

The virtual works done by the damping forces on the two micro-beams and those of the electrical attractions can be written as:

$$\delta W_D^i = -cb \int_0^L \dot{w}_i \delta w_i dx, \tag{9a}$$

$$\delta W_c^i = \int_0^b \int_0^L F_c^i \delta w_i dx dy = \int_0^L \frac{\varepsilon b V_c^2 (-1)^{i+1}}{2(g_c - w_1 + w_2)^2} H_e(x) \delta w_i dx, \tag{9b}$$

$$\delta W_{ele} = \int_0^b \int_0^L F_{ele} \delta w_2 dx dy = \int_0^L \frac{\varepsilon b (V_{dc} + V_{ac} \cos(\Omega t))^2}{2(g_a - w_2)^2} H_e(x) \delta w_2 \, dx. \tag{9c}$$

The variational form of the kinetic energy associated with the upper and the lower micro-beams are given by [27]:

$$\delta K_1 = b \int_0^L \rho_s h_1 \left(\dot{u}_1 \delta \dot{u}_1 + \dot{w}_1 \delta \dot{w}_1 \right) dx + \int_0^L \delta(x - x_0) m_p \left(\dot{w}_1 \delta \dot{w}_1 \right) dx, \tag{10a}$$

$$\delta K_2 = b \int_0^L \left\{ \rho_s h_2 + \rho_p h_p (H_1(x) + H_2(x)) \right\} \left(\dot{u}_2 \delta \dot{u}_2 + \dot{w}_2 \delta \dot{w}_2 \right) dx, \tag{10b}$$

where the dot-superscript denotes differentiation with respect to time t. Also, $\delta_{i\,2}$, $\delta\,(x - x_0)$, and m_p, respectively, refer to the Kronecker delta, Dirac delta function, and mass of the small particle attached to the upper micro-beam. In addition, ρ_i is the density of the ith micro-beam (i = 1,2). As previously stated, the density of the upper micro-beam (i.e., ρ_1) remains constant throughout its thickness. However, the density of the lower micro-beam (i.e., ρ_2) varies throughout its thickness and can be expressed as:

$$\rho = \begin{cases} \rho_p H_1(x) & -(h_p + h_2/2) \le z \le -h_2/2 \\ \rho_s & -h_2/2 \le z \le h_2/2 \\ \rho_p H_2(x) & h_2/2 \le z \le (h_2/2 + h_p) \end{cases} , \tag{11}$$

where ρ_p and ρ_s are the densities of the piezoelectric layers and substrate of the lower micro-beam, respectively. The equations of motion associated with the present system can be obtained by employing Hamilton's principle. This principle for an elastic body can be stated as [27]:

$$\int_{t_f}^{t_i} \left(\delta K_i - \delta U_i + \delta W_{ext}^i \right) \, dt = 0, \tag{12}$$

where δW_{ext}^i (i = 1,2) refers to the virtual works done by the external forces on the ith micro-beam and introduces as follows:

$$\delta W_{ext}^i = \delta W_c^i + \delta W_D^i + \delta_{i2} \, \delta W_{ele}, \tag{13}$$

Substituting Eqs. (3), (9), and (10) into Hamilton's principle in (12), integrating the in-plane equations by part, neglecting the axial accelerations in comparison to the translatory ones and solving the displacement u_i in terms of the deflection W_i for the case of clamped boundary conditions, one gets:

$$\begin{aligned} \int_{t_i}^{t_f} \int_0^L \Big\{ & b\left(\rho_s h_i + \delta_{i1} \, \delta(x - x_0) m_p + \delta_{i2} \, \rho_p h_p (H_1(x) + H_2(x))\right) \ddot{w}_i \, \delta w_i \\ & + c \, \dot{w}_i \, \delta w_i + b \widetilde{N}_i \, w_i^{'} \, \delta w_i^{'} \\ & - b \widetilde{M}_i \, \delta w_i^{''} - \frac{\varepsilon b V_c^2 (-1)^{i+1}}{2(g_c - w_1 + w_2)^2} \, H_e(x) \, \delta w_i \\ & - \frac{\delta_{i2} \, \varepsilon \, b (V_{dc} + V_{ac} \cos(\Omega \, t))^2}{2(g_a - w_2)^2} \, H_e(x) \, \delta w_2 \Big\} dt dx \\ = 0, & \end{aligned} \tag{14}$$

The stress resultants $\widetilde{N}_i$ and $\widetilde{M}_i$ (i = 1,2) introduced in Eq. (14) are defined as:

$$\widetilde{N}_1 = \frac{E_s h_1}{2L} \left(\int_0^L (w_1^{'})^2 dx \right), \quad \widetilde{M}_1 = -\left(\frac{E_s h_1^3}{12} \right) w_1^{''},$$

$$\begin{aligned} \widetilde{N}_2 = \{N + A\} \Big(& - a_1 \, w_2^{''} - a_2 + a_3 \Big\{ \int_0^L \frac{1}{2} (w_2^{'})^2 dx + \int_0^L a_1 \, w_2^{''} \, dx \\ & + \int_0^L a_2 \, dx \Big\} \Big) + B \, w_2^{''} + Np, \end{aligned} \tag{15}$$

$$\begin{aligned} \widetilde{M}_2 = -B \Big(& - a_1 \, w_2^{''} - a_2 + a_3 \Big\{ \int_0^L \frac{1}{2} (w_2^{'})^2 dx + \int_0^L a_1 \, w_2^{''} dx \\ & + \int_0^L a_2 dx \Big\} \Big) - \{M + D\} w_2^{''} + Mp. \end{aligned}$$

where

$$D = \frac{1}{3}E_p\left(h_p^3 + \frac{3}{2}h_p^2 h + \frac{3}{4}h_p h^2\right)(H_1(x) + H_2(x)),\ Np = e_{31}(V_{p1}H_1(x) + V_{p2}H_2(x)), N = E_s h_2,\ M = \frac{E_s h_2^3}{12},\ A = E_p h_p (H_1(x) + H_2(x)),\ B = \frac{1}{2}E_p h_p(h_p + h)(H_1(x) - H_2(x)), \tag{16}$$

$$Mp = \frac{1}{2}e_{31}(h_p + h)(V_{p2}H_2(x) - V_{p1}H_1(x)),\ a_1 = \frac{B}{N+A},\ a_2(x) = \frac{Np}{N+A},\ a_3 = \frac{1}{\{N+A\}\int_0^L \frac{dx}{N+A}}.$$

For convenience, the equations of motion associated with the present system given in Eq. (14) are also normalized. To this end, the following non-dimensional variables are introduced:

$$\widehat{x} = \frac{x}{L},\ \widehat{w}_1 = \frac{w_1}{g_a},\ \widehat{w}_2 = \frac{w_2}{g_a},\ \widehat{t} = \frac{t}{\tau},\ R = \frac{g_c}{g_a}, \tag{17}$$

where

$$\tau = \sqrt{\frac{12\rho_s L^4}{E_s h^2}}, \tag{18}$$

Upon substitution of the non-dimensional quantities given in Eq. (17) into Eq. (14) and dropping the hats, the following normalized equations of motion are obtained:

$$w_1''\delta w_1'' + (1 + \delta(x)\Delta m)\ddot{w}_1\delta w_1 + c_1\dot{w}_1\delta w_1 + \alpha_1\left(\int_0^1 w_1'^2 dx\right)w_1'\delta w_1' - \alpha_2 V_c^2\frac{H_e(x)}{(R - w_1 + w_2)^2}\delta w_1 = 0, \tag{19a}$$

$$\begin{aligned}&\beta_2(\rho_p h_p(H_1(x) + H_2(x)) + \rho_s h_2)\ddot{w}_2\,\delta w_2 + c_2\,\dot{w}_2\,\delta w_2 + \beta_1(\{M + D\} - a_1 B)w_2''\,\delta w_2'' \\ &+ \beta_1\{a_3 B\,\delta w_2'' + g_a a_3\{N + A\}w_2'\,\delta w_2'\}\left\{\frac{g_a L}{2}\int_0^1 (w_2')^2 dx + L\int_0^1 a_1 w_2'' dx + \frac{L^3}{g_a}\int_0^1 a_2\,dx\right\} \\ &- \frac{\beta_1 L^2}{g_a}(Mp + a_2 B)\,\delta w_2'' + \alpha_3\frac{V_c^2 H_e(x)}{(R - w_1 + w_2)^2}\delta w_2 - \alpha_3\frac{(V_{dc} + V_{ac}\cos(\Omega t))^2 H_e(x)}{(1 - w_2)^2}\delta w_2 = 0,\end{aligned} \tag{19b}$$

where the normalized parameters of the system are given by:

$$\Delta m = \frac{m_p}{\rho_s b h_1 L},\quad c_1 = \frac{12\,c\,L^4}{E_s\,b\,h_1^3\,\tau},\quad c_2 = \frac{12\,c\,L^4}{E_s\,b\,h_2^3\,\tau},\quad \alpha_1 = 6\frac{g_a^2}{h_1^2},$$

$$\alpha_2 = \frac{6\,\varepsilon\,L^4}{E_s\,h_1^3 g_a^3},\quad \alpha_3 = \frac{6\,\varepsilon\,L^4}{E_s\,h_2^3\,g_a^3},\quad \beta_1 = \frac{12}{E_s\,h_2^3},\quad \beta_2 = \frac{h_1^2}{\rho_s\,h_2^3}. \tag{20}$$

Also, functions $H_1(x)$, $H_2(x)$, and $H_e(x)$ appeared in Eq. (19) are given below:

$$H_1(x) = H\left(\frac{L_p}{L} - x\right) + H\left(x - \left(\frac{L - L_p}{L}\right)\right), \tag{21a}$$

$$H_2(x) = H\left(x - \frac{(L - L_p)}{2L}\right) + H\left(x - \frac{(L + L_p)}{2L}\right), \tag{21b}$$

$$H_e(x) = H\left(\frac{L_e}{L} - x\right) + H\left(x - \left(\frac{L - L_e}{L}\right)\right). \tag{21c}$$

According to the physics of the mass sensor, where it deflects toward a static position and then oscillates around its static configuration, the deflections of micro-beams are divided into two static and dynamic counterparts. Afterward, since providing exact solutions for the problem at hand is almost impossible [27], an approximate solution will be developed through the Ritz method in the present work. According to the Ritz method, the deflections of micro-beams are discretized as:

$$w_1(x,t) = \sum_{i=1}^{n}\phi_i(x)\,q_{s1,i} + \sum_{j=1}^{N}\phi_j(x)\,q_{d1,j}(t) \tag{22a}$$

$$w_2(x,t) = \sum_{i=1}^{n}\phi_i(x)\,q_{s2,i} + \sum_{j=1}^{N}\phi_j(x)\,q_{d2,j}(t), \tag{22b}$$

where $q_{s1,i}$ and $q_{s2,i}$, are the ith static generalized coordinates associated with the upper and lower micro-beams, respectively. In addition, $q_{d1,j}(t)$ and $q_{d2,j}(t)$ are their corresponding j^{th} dynamic counterparts. Furthermore, the ith linear un-damped mode shape of a clamped beam, which is taken as the ith admissible basis function discretizing the present system of boundary value problems, is given by [30]:

$$\phi_i(x) = (\cos(\beta_i x) - \cosh(\beta_i x)) - \frac{\cos(\beta_i) - \cosh(\beta_i)}{\sin(\beta_i) - \sinh(\beta_i)}(\sin(\beta_i x) - \sinh(\beta_i x)), \tag{23}$$

where β_i is the ith eigenvalue of the clamped beam that can be calculated as $\beta_1 = 4.7300$, $\beta_2 = 7.8532$, and $\beta_3 = 10.9956$ [30]. Next, substituting Eqs. (22) with the corresponding dynamic counterpart eigenmode, on which we would like to focus, into Eqs. (19), integrating the outcomes over the whole dimensionless domain from 0 to 1 and following some straightforward mathematical manipulations, we obtain:

$$\begin{aligned}&\Delta m_j\ddot{q}_{d1,j} + c_1\dot{q}_{d1,j} + \sum_{i=1}^{n} S11_{ij}q_{s1,i} + K11_j q_{d1,j} \\ &+ \alpha_1\left(\int_0^1\left(\sum_{i=1}^{n}\phi_i' q_{s1,i}\right)^2 dx + 2\left\{\sum_{i=1}^{n} S12_{ij}q_{s1,i}\right\}q_{d1,j} + K12_j q_{d1,j}^2\right) \times \left\{\sum_{i=1}^{n} S12_{ij}q_{s1,i} + K12_j q_{d1,j}\right\} \\ &- \alpha_2 V_c^2\left\{INT1_j + INT2_j(q_{d1,j} - q_{d2,j}) + INT3_j\left(q_{d1,j}^2 + q_{d2,j}^2\right) + INT4_j\left(q_{d1,j}^3 - q_{d2,j}^3\right)\right\} = 0\end{aligned} \tag{24a}$$

$$\begin{aligned}&K21_j\ddot{q}_{d2,j} + c_2\dot{q}_{d2,j} + \sum_{i=1}^{n} S21_{ij}q_{s1,i} + K22_j q_{d2,j} - K23_j + \left\{K24_j + \beta_1 g_a\sum_{i=1}^{n} S22_{ij}q_{s2,i} + K25_j q_{d2,j}\right\} \\ &\times\left\{\frac{g_a L}{2}\int_0^1\left(\sum_{i=1}^{n}\phi_i' q_{s2,i}\right)^2 dx + L\int_0^1 a_1\left(\sum_{i=1}^{n}\phi_i'' q_{s2,i}\right)dx + K26 + g_a L\left\{\sum_{i=1}^{n} S23_{ij}q_{s2,i}\right\}q_{d2,j} + K27 q_{d2,j} + K28_j q_{d2,j}^2\right\} \\ &+ \alpha_3 V_c^2\left\{INT1_j + INT2_j(q_{d1,j} - q_{d2,j}) + INT3_j\left(q_{d1,j}^2 + q_{d2,j}^2\right) + INT4_j\left(q_{d1,j}^3 - q_{d2,j}^3\right)\right\}\end{aligned}$$

$$-\alpha_3(V_{dc}+V_{ac}\cos(\Omega t))^2\left\{INT5_j+INT6_jq_{d2,j}+INT7_jq_{d2,j}^2+INT8_jq_{d2,j}^3\right\}=0 \tag{24b}$$

where all the introduced coefficients in this equation are given in Appendix A. It is notable that the static configuration of the present system under the action of the electrical actuations can be determined by neglecting the time-dependent terms in Eqs. (24). Then, having the static configuration of the system, the dynamic equations associated with the present system can simply be obtained around the pre-determined static configuration.

3. Results and discussions

3.1. Static analysis

As mentioned earlier, the deformations of the upper and lower micro-beams are divided into two static and dynamic counterparts induced by the application of DC and AC voltages, respectively. The static configuration of the system under the action of electrostatic excitation can be obtained by neglecting the time-dependent terms in Eqs. (24). It is worth mentioning that the resulting algebraic equations will be solved numerically through the use of the Newton-Raphson procedure [31].

Before going through further analysis of the system, the present static findings need to be validated. To this end, an electrostatically coupled system without the piezoelectric layers is first considered (i.e., the properties related to the piezoelectric layers are set to zero). Table 1 provides the geometric and material properties of the electrostatically coupled system. Also, the electrostatic coupling voltage between the two micro-beams is set to $V_c = 10$ V. It should be noted that the thicknesses of the upper and lower micro-beams are assumed to be the same in this case. Fig. 2 shows the equilibrium path of the lower micro-beam versus the applied DC voltage. This figure compares the present findings with the results obtained from finite element simulation as well as those published in Ref. [23]. As seen, the present static findings are in excellent agreement with those reported by Lyu et al. [23] and also the results obtained from FE simulations performed in COMSOL Multiphysics commercial software [25].

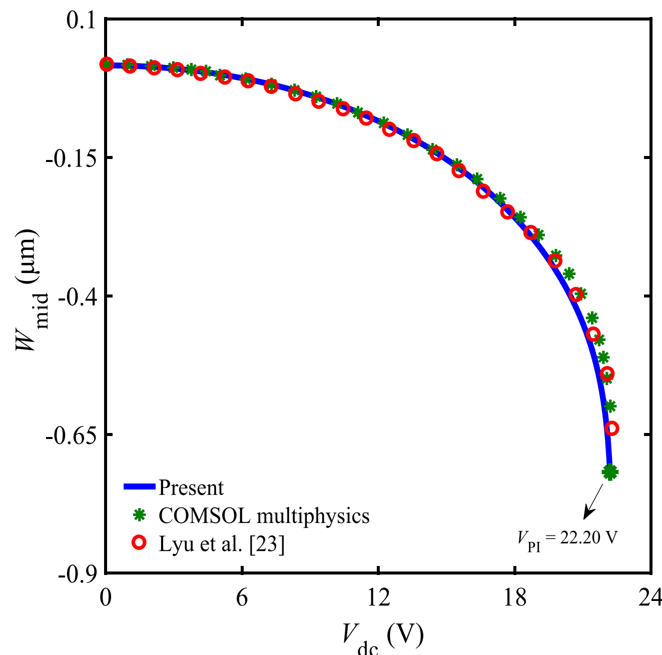

Fig. 2. Equilibrium path of the lower micro-beam for a system with properties presented in Table 1 and $V_c = 10$ V.

Fig. 3 illustrates the 3-D FE model caried out in COMSOL Multiphysics [25]. This simulation was performed by employing the electromechanical forces in the multiphysics menu, which can combine the physics of solid mechanics and electrostatics. The mechanical constraints of the system were established in the physics of solid mechanics by defining micro-beams as linear elastic materials with fixed-end constraints. Furthermore, the electrodes on micro-beam surfaces were selected as volume terminals in the physics of electrostatic to apply the electrostatic attraction between the two micro-beams. It is worth mentioning that, since the electrostatic actuation between the two micro-beams is only applied over the electrode areas, these regions are shown in different colors in Fig. 3. In addition, to discretize the micro-beams and the air gaps between them the tetrahedral elements were selected. Furthermore, the highly nonlinear Newton–Raphson procedure was employed as the solution methodology.

In addition to the validation provided earlier, it is also necessary to validate the present findings for a system subjected to piezoelectric excitation. To this end, a single micro-beam equipped with two piezoelectric layers is considered. It is worth mentioning that the effect of the electrostatic coupling between the two resonators has been neglected by setting $V_c = 0$ in this comparison. The geometric and material properties of this bimorph micro-beam are given in Tables 2 and 3. It is notable that the upper and lower piezoelectric layers are both excited by the same voltage. Fig. 4 illustrates the variation of the pull-in voltage versus the piezoelectric voltage. The results are compared and validated by those available in the literature [32]. It can be seen that the present findings are in good agreement with those obtained by Rezazadeh et al. [32].

Consider an electrostatically coupled system with geometric and material properties listed in Tables 4 and 5. To study the combined influences of the piezoelectric excitation and the electrostatic coupling between the two micro-beams, Fig. 5 demonstrates the variation of the system pull-in voltage versus the piezoelectric voltage for different values of the electrostatic coupling voltages. It should be noted that the upper and lower micro-beams are assumed to be identical, and the piezoelectric layers are excited by the same voltage. Based on the results presented in Fig. 5, it can be observed that, increasing the piezoelectric excitation at the same coupling voltage decreases the pull-in voltage of the system. The reason behind this observation is that increasing the piezoelectric excitation causes a compressive force to be applied on the lower micro-beam and so reduces its stiffness. Another conclusion that can be drawn from Fig. 5 is that the electrostatic coupling has a significant impact on the occurrence of pull-in instability, so that increasing the coupling voltage increases the pull-in threshold of the system. This is due to the fact that increasing the coupling voltage can increase the attraction between the upper and lower micro-beams, which needs to be compensated by increasing the DC voltage. Therefore, as observed, the utilization of piezoelectric and electrostatic actuations between the micro-beams offers greater control over the onset of the pull-in instability as well as the static behavior of the present system.

3.2. Eigenvalue loci veering analysis

This section explores the influence of the piezoelectric excitation and the electrostatic coupling between the two micro-beams on the veering phenomenon. As mentioned in the introduction section, introducing a slight disorder to one of the resonators unbalances the system, leading to the occurrence of the mode-localization phenomenon. To find the balance state of a tunable system, one should investigate the variation of the system's eigenvalues with respect to the disorder parameter. The eigenvalue problem associated with the present system can simply be obtained by neglecting the damping terms and then linearizing the reduced governing equations of motion in Eq. (24) around its static configuration determined in the previous section.

As mentioned earlier, there exist no previous studies dealing with the influence of piezoelectric excitation on the veering phenomenon. Hence,

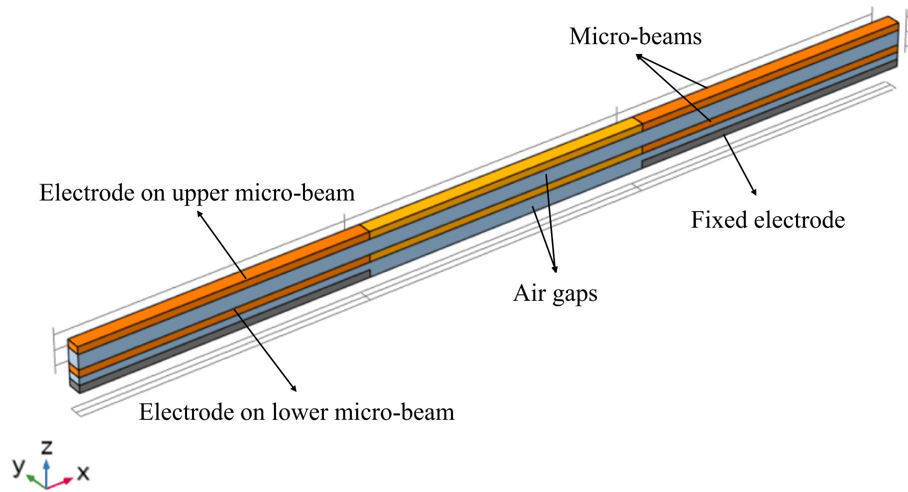

Fig. 3. 3-D model created in COMSOL Multiphysics software [25].

Table 1
Geometric and material properties of the electrostatically coupled system studied in Ref. [23].

L(μm)	b(μm)	h(μm)	g_c(μm)	g_a(μm)	E(GPa)	ρ(kg/m^3)
210	4	1	2	1	169	2320

Table 2
Geometric and material properties of the substrate associated with the system studied in Ref. [32].

L(μm)	b(μm)	h(μm)	g_a(μm)	E(GPa)	ρ(kg/m^3)
350	50	3	1	169	2331

Table 3
Geometric and material properties of the piezoelectric layers associated with the system studied in Ref. [32].

L(μm)	b(μm)	h(μm)	E(GPa)	ρ(kg/m^3)	e_{31}
350	50	0.01	78.6	7500	−9.29

to verify the accuracy of the findings, neglecting the influence of piezoelectric excitation, the present system with properties listed in Table 1 is considered again. The electrostatic actuation applied to the lower micro-beam and the coupling voltage between the two micro-beams are set to $V_{dc} = 1$ V and $V_c = 10$ V, respectively. Fig. 6(a) and 6(b) illustrate the variation of the system's natural frequencies versus the thickness of the lower micro-beam as the disorder parameter where the second and third eigenmodes of the micro-beams are coupled to each other, respectively. In this figure, the Ω_1 and Ω_2 represent the first and second eigen frequencies of the whole system. This figure also compares the present findings by those reported by Lyu et al. [23] as well as three-dimensional (3-D) FE simulations carried out in COMSOL. It can be observed from Fig. 6 that the present findings align more closely with the FE results than those presented by Lyu et al. [23]. To ensure the accuracy of the present Ritz and FE models, Fig. 7 provides another comparison between the present findings and those published by Zhao et al. [24]. As this figure depicts, both the present Ritz and FE results are in excellent agreement with those reported in the literature [24]. So, it can generally be concluded that the present work provides more accurate results in comparison to those reported in Ref. [23].

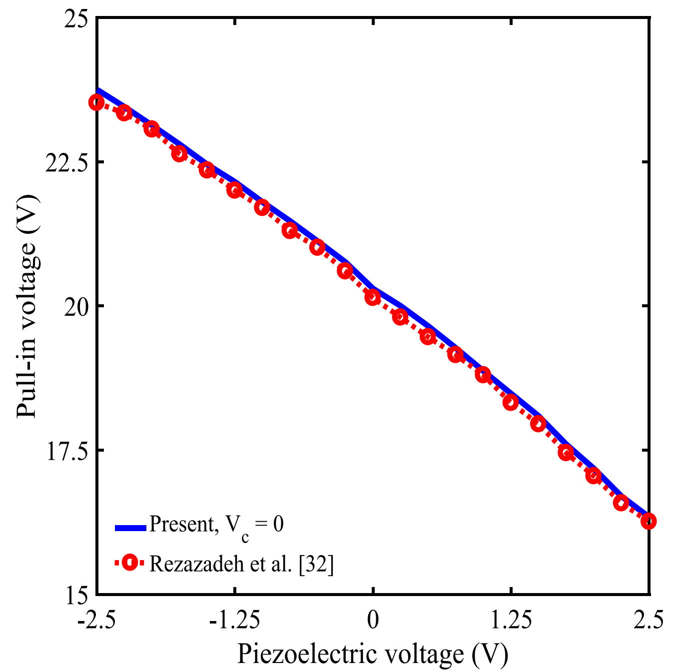

Fig. 4. Variation of the pull-in voltage versus piezoelectric excitation for a single bimorph micro-beam with properties presented in Tables 2 and 3.

Table 4
Geometric and material properties of the electrostatically coupled micro-beams investigated in Fig. 5.

L(μm)	b(μm)	h(μm)	g_c(μm)	g_a(μm)	E(Gpa)	ρ(kg/m^3)
210	4	1	2	1	169	2320

Table 5
Geometric and material properties of the piezoelectric layers associated with the system investigated in Fig. 5.

L(μm)	b(μm)	h(μm)	E(GPa)	ρ(kg/m^3)	e_{31}
70	4	0.005	78.6	7500	−9.29

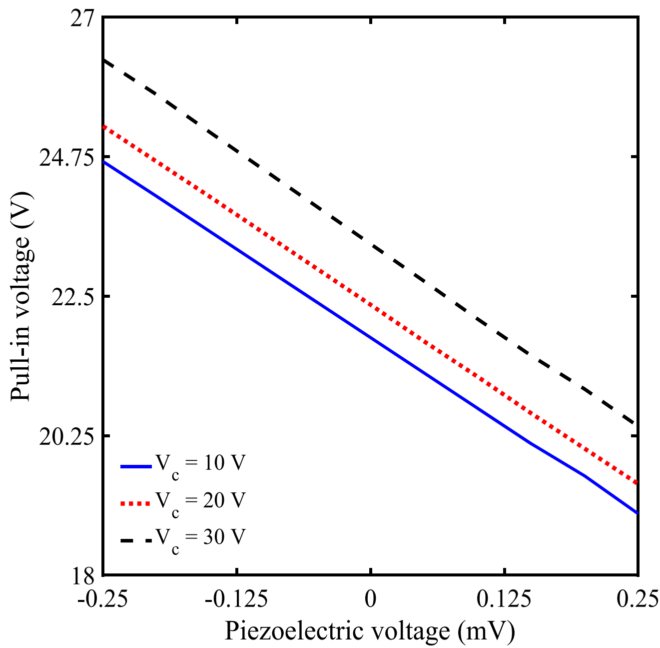

Fig. 5. Variation of the pull-in threshhold versus the piezoelectric excitation for different values of the coupling voltages. The system properties are listed in Tables 4 and 5.

To investigate the influence of the electrostatic coupling between the two micro-beams on the veering phenomenon, the present system with properties given in Tables 4 and 5 is considered. The upper and lower micro-beams are assumed to have similar thicknesses and a similar voltage across the piezoelectric layers is applied. In this study, the third eigenmodes of the micro-beams are coupled with each other, and V_{dc} is set to 1 V. Fig. 8 shows the variation of the natural frequencies of the system versus the piezoelectric voltage as the disorder parameter for different coupling voltages. As this figure depicts, the value of the coupling voltage seriously affects the occurrence of the veering phenomenon so that it happens only in systems with a small coupling voltage. To investigate this issue with more detail, Table 6 provides the eigenvector values for the veering point as well as for some points prior to and beyond this point. It is worth mentioning that the upper to lower micro-beam mid-point deflection ratios are picked as the representative of the eigenvector value. In addition, the first digit in the superscript of the parameters presented in Table 6 denotes the micro-beam number. Specifically, the superscripts 1 and 2 refer to the upper and lower micro-beams, respectively. The second digit indicates the system mode number, where superscripts 1 and 2 represent the first and second mode-shape of the coupled system, respectively. It is worth noting that, as shown in Table 6, the absolute eigenvector values coincide when the veering phenomenon occurs, and this phenomenon occurs only in systems with weak couplings as expected [16].

As mentioned earlier, the results shown in Table 6 reveal that despite the strongly coupled system (i.e., the case with $V_c = 35$V), the absolute eigenvector values become identical at the veering point. In addition, getting away from the veering point drastically changes these values just in the case of weakly coupled systems. This means that both the vibration modes are excited identically at the veering point (the so-called balance state) and taking distance from this point results in the localization of the vibration mode around one of the resonators (the one without the disorder), and suppressing the other one's oscillations only in the weakly coupled system. This localization phenomenon is the sensing principle of mode-localized mass micro-sensors [33].

As previously discussed, any factor influencing the stiffness of the resonator has the potential to alter the position of the veering point, serving as a means to tune mode-localized mass sensors. Given that electrical actuation can only decrease the structure's stiffness, and consequently lacks tunability, the notion of employing piezoelectric actuation arises. Piezoelectric actuation, capable of both increasing and decreasing resonator stiffness, presents itself as a viable solution. It is worth noting that utilizing piezoelectric actuation can offer additional degrees of freedom for tuning the sensor. Regarding this issue, Fig. 9 investigates the combined effects of the piezoelectric and electrostatic actuations on the eigenvalues loci of the system. As this figure depicts, increasing the DC voltage changes the balance condition of the system and shifts the veering point to the left. The reason behind this observation is that applying electrostatic actuation reduces the stiffness of the structure, which needs to be compensated by applying a tensile force

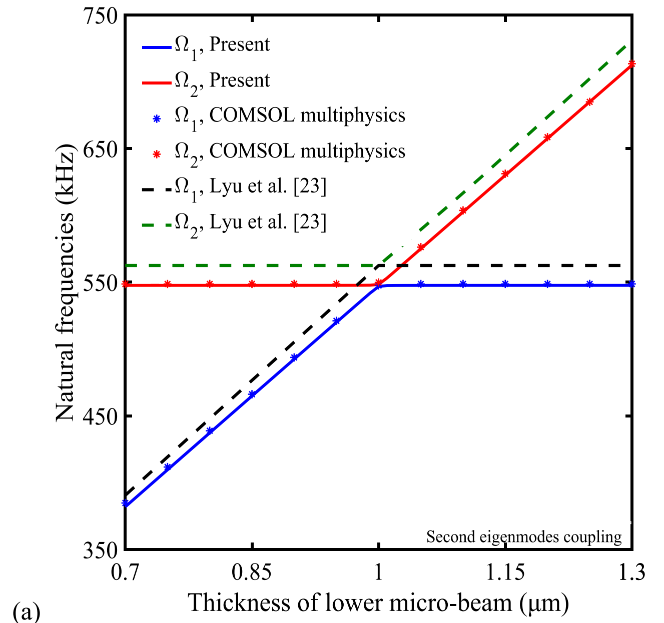

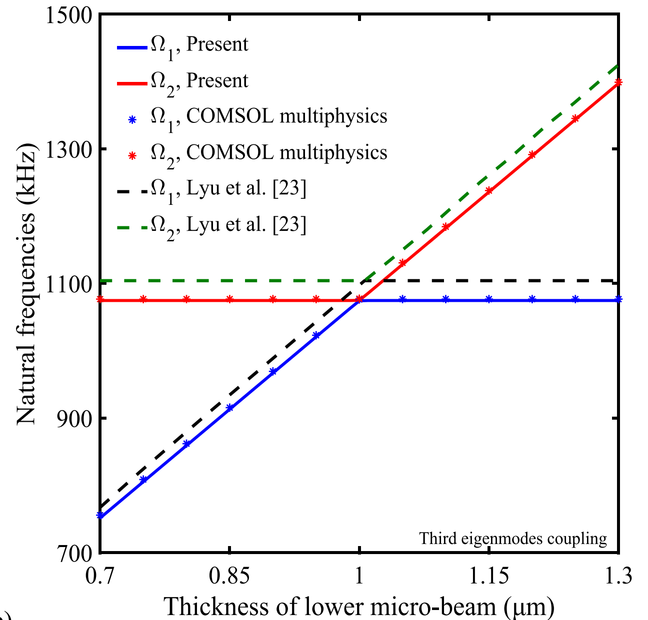

Fig. 6. Comparison of the first and second system's natural frequencies obtained by the present Ritz and FE models as well as those obtained by Lyu et al. [23], when (a) the second and (b) the third eigenmodes of the micro-beams are coupled with each other.

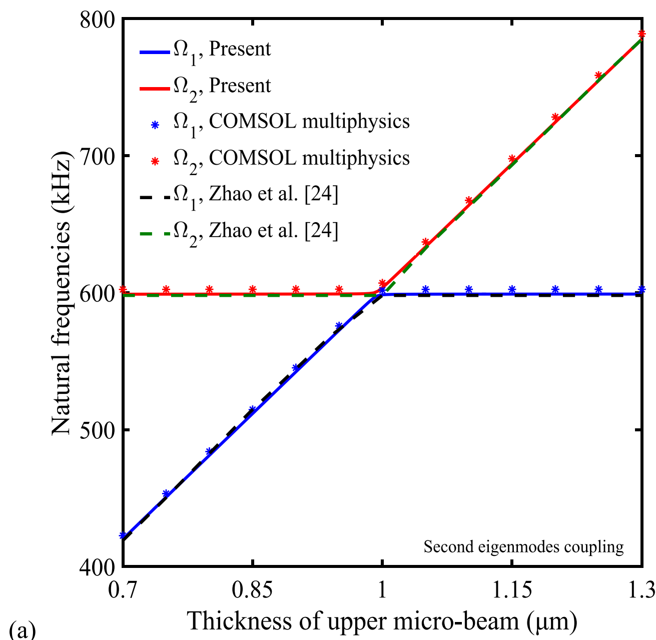

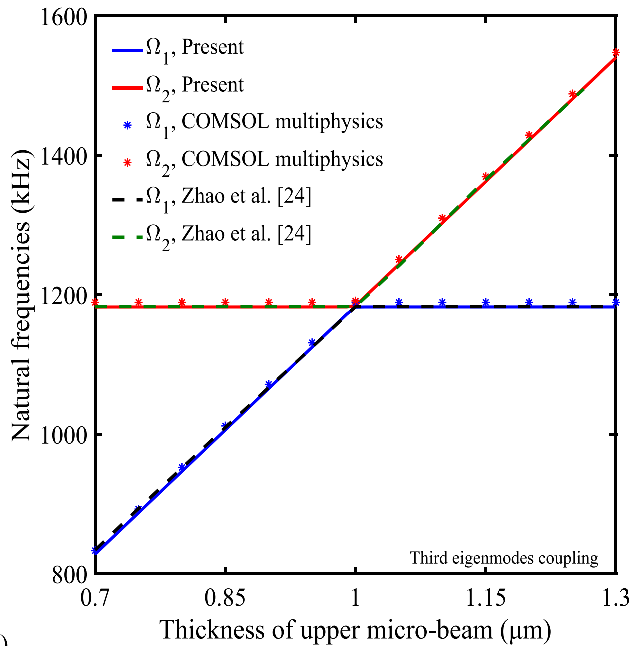

Fig. 7. Comparison of the first and second system's natural frequencies obtained by the present Ritz and FE models as well as those obtained by Zhao et al. [24], when (a) the second and (b) the third eigenmodes of the micro-beams are coupled with each other.

through increasing the piezoelectric excitation in the inverse direction.

As another investigation, the influence of the initial gaps between the fixed and movable electrodes (i.e., g_a and g_c) on the occurrence of the veering phenomenon is better to be studied. It is notable that, according to Eq. (7), the electrical attraction between each two electrodes is inversely proportional to the square of the initial gap between them. So, it is completely expectable that increasing the initial gaps results in weakening the electrical attraction between the electrodes. However, to have a comprehensive point of view about how changing these gaps affects the occurrence of the veering phenomenon, Fig. 10 illustrates the eigenvalue loci of the present system for different values of g_a and g_c. The voltage applied to the piezoelectric layers is set to V_p = -50 mV and the

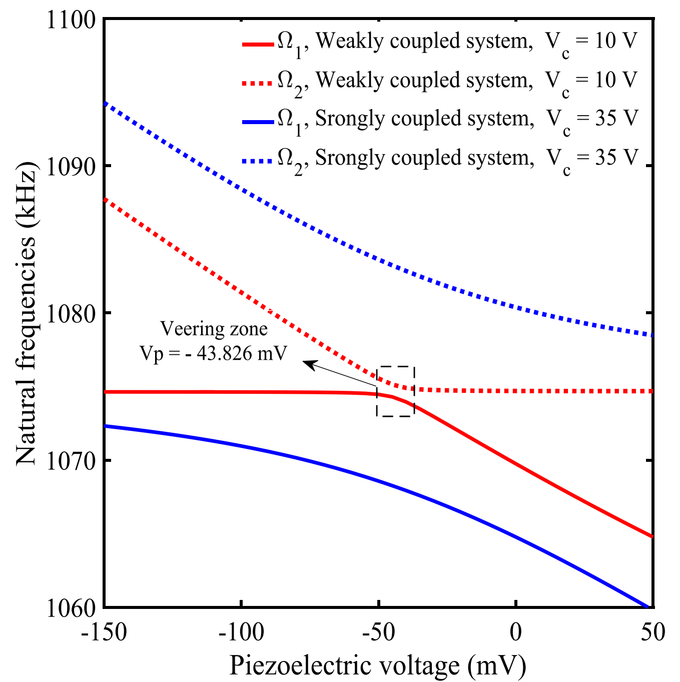

Fig. 8. Eigenvalue loci of the present electrostatically coupled system under different coupling voltages. The properties are assumed to be as those given in Tables 4 and 5 and V_{dc} = 1 V.

Table 6
Eigenvectors associated with different points of the eigenvalue loci presented in Fig. 8.

V_p(mV)	V_c = 10 V		V_c = 35V	
	$W_{mid}^{11}/W_{mid}^{21}$	$W_{mid}^{12}/W_{mid}^{22}$	$W_{mid}^{11}/W_{mid}^{21}$	$W_{mid}^{12}/W_{mid}^{22}$
− 132	−26.5032	0.0383	−2.6118	0.3891
− 88	−12.9656	0.0784	−1.7668	0.5751
− 43.826	−1.0080	1.0081	−1.1079	0.9172
0	12.0852	−0.0841	−0.6956	1.4608
44	23.2593	−0.0437	−0.4714	2.1555

other geometric and material properties of the system remain unchanged as those previously given in Tables 4 and 5. As Fig. 10 shows, increasing the value of the initial gap between the fixed electrode and the lower micro-beam reduces the influence of the electrical interaction between them which can partially be compensated by increasing the applied voltage (i.e. V_{dc}). This leads to shifting the position of the veering point to the right (see Fig. 10(a)). Additionally, it can be observed that despite the coupling voltage (i.e. V_c), increasing the initial gap between the two micro-beams (i.e. g_c) results in weakening the electrical coupling between them and so strengthening the occurrence of the veering phenomenon. That is, the lower the coupling voltage, the smaller the initial gap (see Fig. 10(b), 10(d) and 10(f)). Finally, it should be indicated that once the initial gaps of the system are selected, the proper values for the applied voltages, as the design parameters of the system, should be obtained to have a sufficiently strength veering phenomenon required for having a mode-localized mass sensor.

3.3. Dynamic analysis

As the present system is nonlinear, its dynamic behavior cannot accurately be predicted through the linear eigenvalue loci analysis provided in the previous section. Therefore, this section is devoted to the dynamic analysis of the present system. To this end, since studying a dynamical system in the frequency domain can provide a more

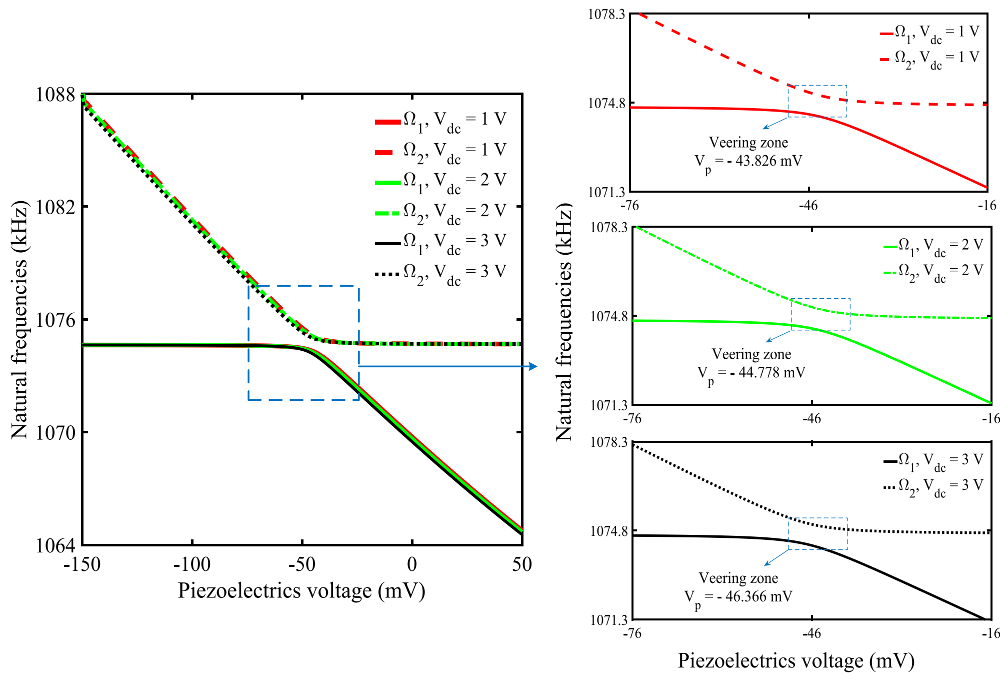

Fig. 9. Combined effects of the piezoelectric and electrostatic excitations on the third eigenvalues loci of the present system. The system properties are given in Tables 4 and 5 and $V_c = 10$ V.

comprehensive point of view about its behavior in comparison to focusing on its time response, the method of harmonic balance [34] is adopted here to obtain the frequency response function associated with the present system (see Appendix B for more details). For this purpose, the present electrostatically coupled system with properties presented in Tables 4 and 5 is considered again. Also, the AC and coupling voltages are set to $V_{ac} = 20$ mV and $V_c = 10$ V, respectively. It is worth mentioning that to calculate the damping force between two micro-beams, the quality factor is set to $Q = 1/2\zeta = 8000$, where ζ is the damping ratio. It is assumed that the voltages applied across the piezoelectric layers are the same, and the third eigenmodes of the micro-beams are coupled with each other. It is worth noting that the system is actuated at its balanced state. Hence, the piezoelectric and DC voltages are set to the values corresponding to the veering point shown in Fig. 9.

Fig. 11 represents the frequency response curves associated with the upper and lower micro-beams under different combinations of the piezoelectric and electrostatic actuations. As observed, the curves contain two peaks around the natural frequencies of the system each of which refers to its corresponding mode of vibration. In addition, the results indicate that increasing the values of the applied DC voltage, leading to an increase in the piezoelectric excitation corresponding to the system's veering point amplifies the amplitudes of both the upper and lower micro-beams' vibrations. This causes the system to exhibit more pronounced nonlinearity.

3.4. Sensitivity

As mentioned earlier, the main objective of the present work is to increase the sensitivity of mode-localized mass micro-sensors by introducing piezoelectric excitation to these systems. Therefore, this section aims to investigate the influence of equipping the lower electrode with thin-film piezoelectric patterns on the sensitivity of the device. The sensitivity of resonant mass sensors can generally be determined by calculating either the resonance frequency position shift or the vibrational amplitude change of the device before and after the attachment of the added mass [31]. It has been shown that measuring the change in the vibrational amplitude can provide a better representation of the system sensitivity in comparison to calculating the shift in the resonance frequency position for a mode-localized mass sensor [35]. Therefore, the amplitude-based method is employed here to calculate the sensitivity of the present mass sensor. The sensitivity metric based on this method is defined as [23]:

$$S_j^a = \left| \left(\frac{W_{2,j}}{W_{1,j}} - \frac{W_{2,j}^0}{W_{1,j}^0} \right) \Big/ \frac{W_{2,j}^0}{W_{1,j}^0} \right| \Delta m \tag{25}$$

where $j = 1, 2$ refers to the 1st and 2nd mode of the coupled system, $W_{1,j}^0$ and $W_{2,j}^0$ are the amplitude of the upper and lower micro-beams at the corresponding balanced state, and $W_{1,j}$ and $W_{2,j}$ are those associated with the case with the added mass.

Before going through the sensitivity analysis of the present system, the influence of the added mass on the frequency response curves of the micro-beams will be investigated. To this end, the values of the DC and piezoelectric voltages are taken as $V_{dc} = 3$ V and $V_p = -46.366$ mV, which correspond to the veering point of the present system. The position of the applied mass on the upper micro-beam is set to $x_0 = 0.208$ as it may present the maximum sensitivity of micro-beams whose third eigenmodes are weakly coupled with each other [24]. This is due to the fact that this position is related to the maximum amplitude corresponding to the third mode shape of the clamped micro-beam. Fig. 12 depicts the frequency responses of the upper and lower micro-beams under different values of the added mass. As observed, the system's resonance frequencies are very close to each other at the balance state (i.e., when there exists no added mass). Thus, when the system is excited by an excitation frequency within the system's resonance zone, both the upper and lower micro-beams simultaneously oscillate with high amplitudes. Assuming the excitation frequency remains unchanged, the case with the introduced small mass to the upper micro-beam is considered. It can be observed that introducing a small mass shifts the position of the resonance frequencies. However, since the coupling is so weak, the lower frequency, which is very close to that of the upper micro-beam with the added mass, is shifted more than the higher one, which is very close to that of the lower micro-beam. Therefore, the higher resonance frequency of the system remains in the vicinity of the excitation frequency and the other one moves away from it. So, the

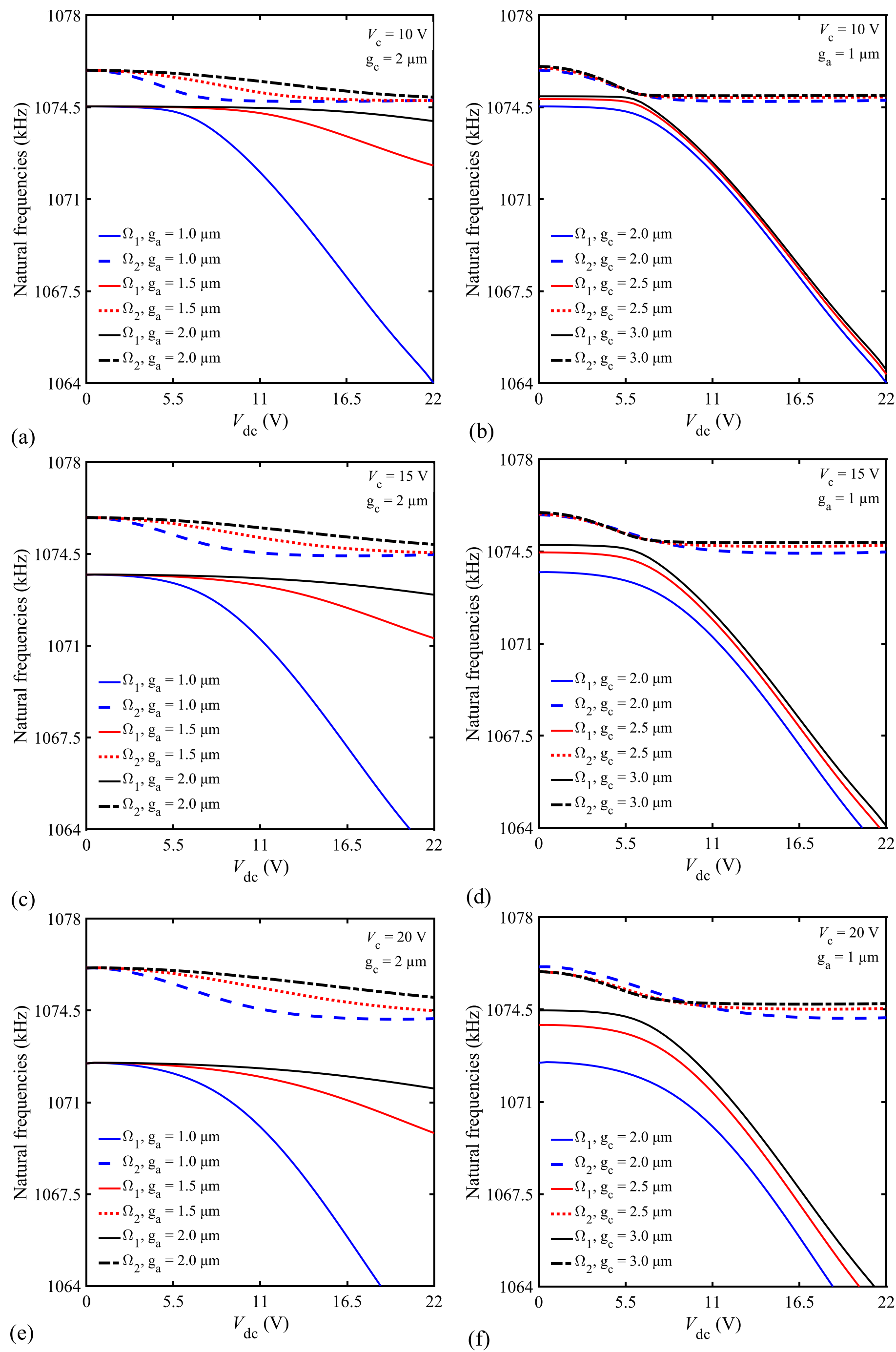

Fig. 10. Eigenvalue loci of the present electrostatically coupled system for different values of g_a and g_c. The value of the piezoelectric is set to V_p = -50 mV and the other properties are assumed to be as those given in Tables 4 and 5.

vibration amplitude of the upper micro-beam is suppressed and considering the input energy of the system does not change, the vibration amplitude of the lower micro-beam is drastically increased. This means that the vibration mode is strongly localized around the resonator on which the disturbance is not introduced. This is the main concept of the mode-localization phenomenon, where attaching a small mass to the upper micro-beam clearly suppresses the amplitude of its vibration.

Particularly, as Fig. 12 demonstrates, introducing the added mass decreases the maximum vibration amplitude of the upper micro-beam around its 2nd system's mode from 0.01158 µm to 0.00628 µm. At the same time, the maximum vibration amplitude of the lower micro-beam around the same mode is increased from 0.011176 µm to 0.02191 µm, which results in the increase of the nonlinear behavior of this micro-beam. This means that the vibration modes of the unbalanced system are strongly localized around the lower micro-beam, which causes an increase in its vibration amplitude and its nonlinear behavior. This drastic change in the vibration amplitude of both micro-beams is the main sensing principle adopted in mode localized mass micro-sensors.

Following the present investigation, the sensitivity of the system under various combinations of piezoelectric and electrostatic actuations needs to be examined. To this end, three different values of the DC voltages and their corresponding piezoelectric voltages that keep the system at its balance state are considered again (see Fig. 9). The position of the applied mass is also set to $x_0 = 0.208$. Fig. 13 presents the relative

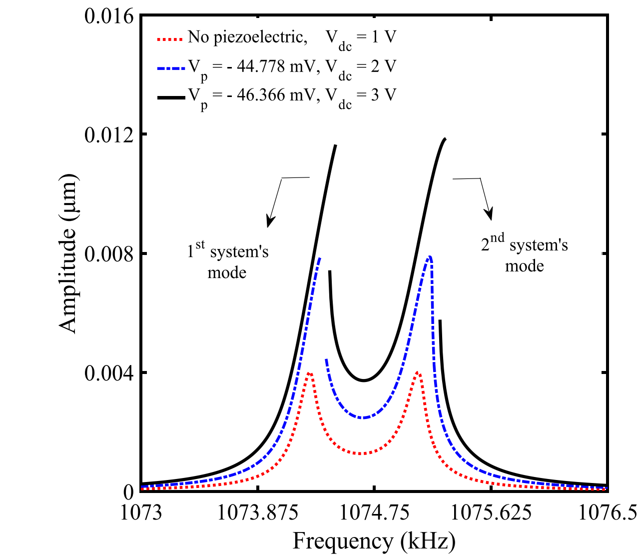

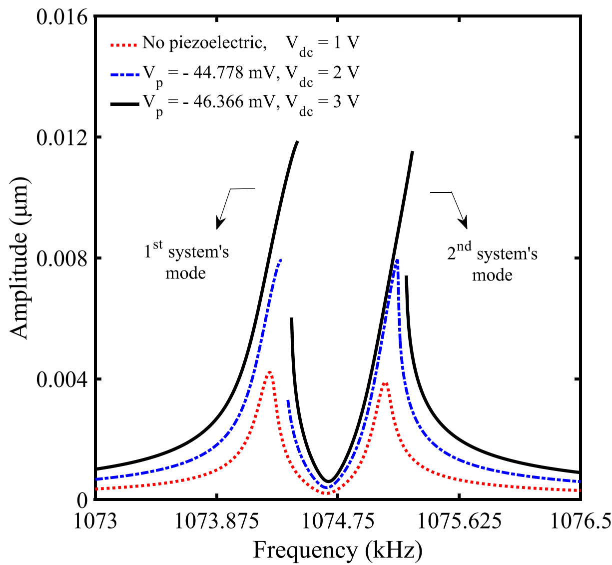

Fig. 11. Frequency responses for the (a) upper and (b) lower micro-beams under different combinations of the piezoelectric and electrostatic actuations when the third eigenmodes of the micro-beams are coupled with each other. The system properties are set to those given in Tables 4 and 5, also $V_{ac} = 20$ mV.

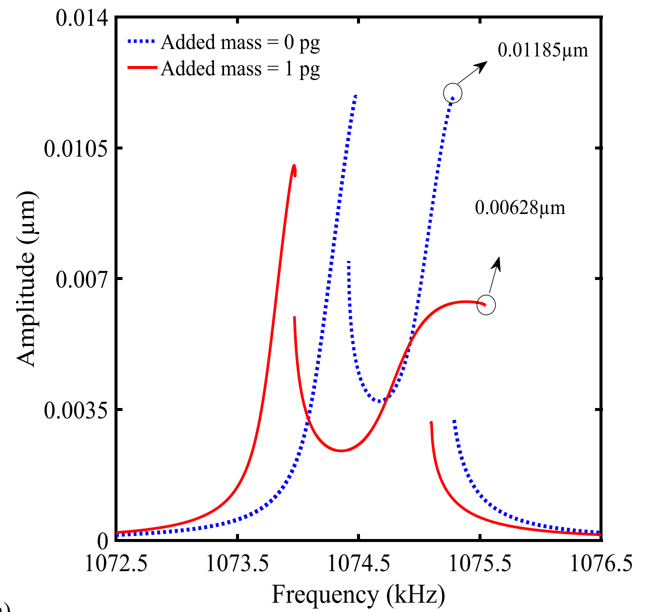

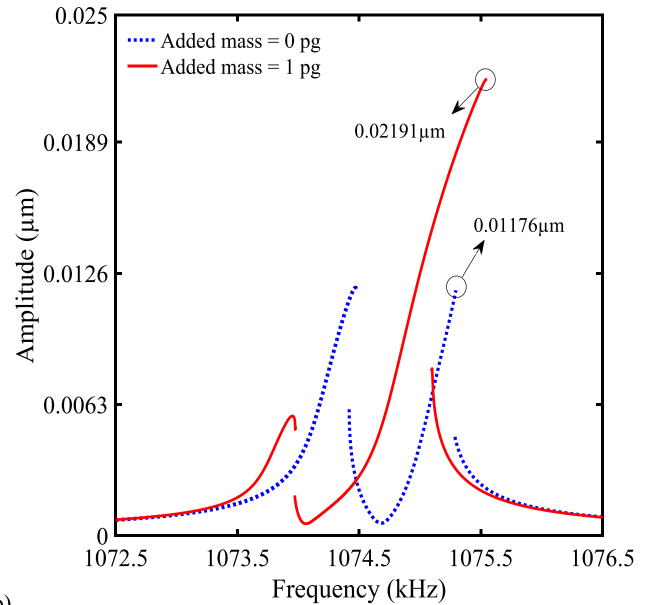

Fig. 12. Frequency responses of the (a) upper and (b) lower micro-beams after adding a mass when the third eigenmodes of the micro-beams are coupled with each other. The system properties are set to those presented in Tables 4 and 5 with $V_{dc} = 3$ V and $V_p = -46.366$ mV.

shift of the amplitude associated with the 1st and 2nd vibration modes of the whole system for the different combinations of the piezoelectric and DC voltages mentioned above. According to Fig. 13, increasing the added mass values has a greater impact on the relative amplitude shift corresponding to the 2nd system's vibration mode in comparison to the first one. Additionally, despite the 1st system's mode, the findings associated with the 2nd system's mode are improved drastically when piezoelectric excitation is introduced. Therefore, the sensitivity of the device around the 2nd system's vibration mode is considered as the sensing approach. To this end, Table 7 presents the sensitivity of the system under various combinations of the piezoelectric and DC voltages when the added mass to the upper micro-beam is 1 pg. Upon comparing the findings associated with the present system with those of the system without piezoelectric layers, it is evident that the sensitivity can be further enhanced by employing piezoelectric excitation. In this regard, the sensitivity of mode-localized mass micro-sensors without piezoelectric layers is 111.7309 % per pg. However, by setting the DC voltage to 3 V and adjusting piezoelectric excitation, the sensitivity reaches a value of 243.0497 % per pg. This implies that the sensitivity is enhanced by more than two times compared to the non-adjustable system without piezoelectric layers. Therefore, due to the capability of the piezoelectric excitation to tune the stiffness of the system and its effect on the increase of the system sensitivity, employing adjustable piezoelectric-based mode-localized mass sensors in comparison to the traditional ones is highly recommended.

4. Concluding remarks

The main objective of this study was to introduce a new generation of high-sensitive piezoelectric-based mode-localized mass micro-sensors.

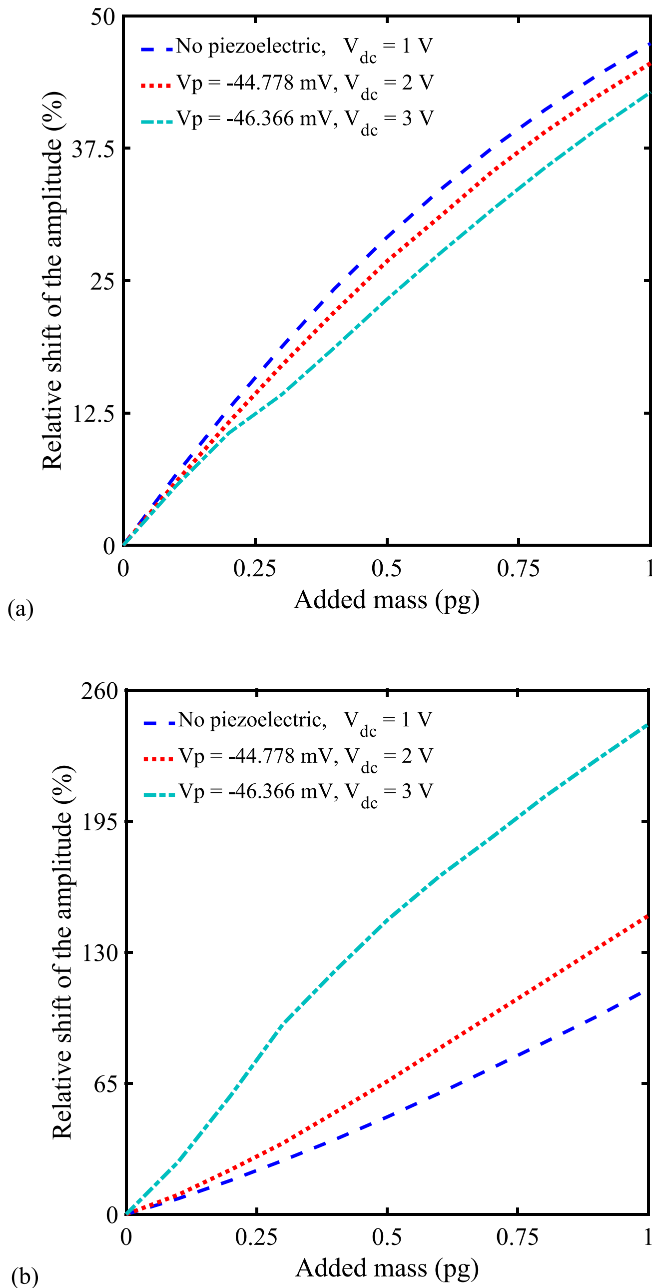

Fig. 13. The relative shift of the amplitude associated with the (a) 1st and (b) 2nd system's mode under different combinations of piezoelectric and electrostatic actuations when the third eigenmodes of the micro-beams are coupled with each other. The system properties are given in Tables 4 and 5.

Table 7
The sensitivity of the present system under various combination of the piezoelectric and DC voltages. Added mass is set to 1 pg.

	No piezoelectric	$V_p = -44.778$ mV	$V_p = -46.366$ mV
	$V_{DC} = 1$ V	$V_{DC} = 2$ V	$V_{DC} = 3$ V
Sensitivity (% per pg)	111.7309	148.0727	243.0497

To this end, a system consisting of two electrostatically coupled micro-beams was considered where the lower one was equipped with a pattern of piezoelectric layers. The nonlinear reduced equations of motion associated with the introduced tunable system were obtained by employing Hamilton's principle together with the Ritz discretization procedure. Linearizing the reduced equations of motion around the static configuration of the system, the veering phenomenon associated with its eigenvalue loci was investigated. Nonlinear dynamics of the proposed system was also assessed by adopting the harmonic balance method. The accuracy of the present findings for the static and eigenvalue analyses were compared and successfully validated by those available in the literature, as well as the results obtained through 3-D finite element simulations performed in COMSOL Multiphysics commercial software. The main conclusions of the present study are summarized below:

- It was observed that piezoelectric excitation, as a mechanism that can both decrease and increase the stiffness of the structure, provides more degrees of freedom than the electrical attraction, which can only decrease the micro-beam stiffness, to tune mode-localized mass micro-sensors.
- It was found that the electrostatic coupling between the lower and upper micro-beams has a significant impact on the occurrence of the pull-in instability associated with lower micro-beam. That is, increasing the electrostatic coupling between the two micro-beams increases the pull-in threshold of the system. The reason behind this observation is that applying electrostatic coupling increases the attraction between the upper and lower micro-beams, which needs to be compensated by increasing the DC voltage between the lower resonator and the fixed electrode underneath it.
- It was observed that the occurrence of the veering phenomenon seriously depends on the value of the initial gap between the movable electrodes as well as the coupling voltage applied between them. That is, only systems with small electrical coupling can incident the veering phenomenon.
- The results revealed that increasing the gap between the lower micro-beam and the fixed electrode shifts the position of the veering point to the right.
- It was found that applying a positive piezoelectric voltage reduces the micro-beam stiffness via the application of a compressive force and a negative one increases it. Therefore, it can be said that piezoelectric excitation can play a crucial role in tuning the balance state of the proposed mode-localized mass micro-sensor.
- It was seen that the attachment of a small mass has a significant impact on the vibration amplitude of both the upper and lower micro-beams. That is, introducing a small particle to the upper micro-beam results in a significant suppression of its vibration amplitude, causing the vibration modes to be localized around the lower micro-beam. This substantial alteration in vibration amplitude is regarded as the key sensing principle of mode-localized mass sensors.
- It was observed that the sensitivity of the sensor is improved by more than two times when compared to traditional mode-localized mass micro-sensors without piezoelectric layers. Therefore, utilizing the piezoelectric excitation in mode-localized mass sensors not only can introduce ultra-sensitive devices but also this approach can provide more degrees of freedom to tune the system.

CRediT authorship contribution statement

Hossein Ali Alam-Hakkakan: Methodology, Software, Validation, Writing – original draft. **Amir Reza Askari:** Conceptualization, Methodology, Software, Supervision, Validation, Writing – original draft, Writing – review & editing. **Masoud Tahani:** Supervision, Writing – review & editing.

Declaration of competing interest

The authors declare that they have no known competing financial

interests or personal relationships that could have appeared to influence the work reported in this paper.

Data availability

Data will be made available on request.

Appendix A

The coefficients appearing in Eqs. (24) are defined as:

$$\Delta m_j = 1 + \phi_j(x_0)\phi_j(x_0)\Delta m,\ \ K11_j = \int_0^1 \left(\phi_j''\right)^2 dx,\ \ K12_j = \int_0^1 \left(\phi_j'\right)^2 dx, \tag{A1}$$

$$K21_j = \int_0^1 \beta_2\left(\rho_p h_p (H_1(x) + H_2(x)) + \rho_s h_2\right)\phi_j^2 dx,\ \ K22_j = \beta_1 \int_0^1 \{(M + D) - a_1 B\}\left(\phi_j''\right)^2 dx$$

$$K23_j = \frac{\beta_1 L^2}{g_a}\int_0^1 (Mp + a_2 B)\phi_j'' dx,\ \ K24_j = \beta_1 \int_0^1 a_3 B\phi_j'' dx,\ \ K25_j = \beta_1 g_a \int_0^1 a_3 \{N + A\}\left(\phi_j'\right)^2 dx,$$

$$K26 = \frac{L^3}{g_a}\int_0^1 a_2\, dx,\ \ K27 = L\int_0^1 a_1\, \phi_j''\, dx,\ \ K28_j = \frac{g_a L}{2}\int_0^1 \left(\phi_j''\right)^2 dx$$

$$S11_{ij} = \int_0^1 \phi_i''\phi_j'' dx,\ \ S12_{ij} = \int_0^1 \phi_i'\phi_j' dx,\ \ S21_{ij} = \int_0^1 \beta_1(\{M + D\} - a_1 B)\phi_i''\phi_j'' dx,$$
$$S22_{ij} = \int_0^1 a_3\{N + A\}\phi_i'\phi_j' dx,\ \ S23_{ij} = \int_0^1 \phi_i'\phi_j' dx \tag{A2}$$

$$INT1_j = \int_0^1 \frac{\phi_j H_e(x) dx}{\left(R - \sum_{i=1}^n \phi_i q_{s1,i} + \sum_{i=1}^n \phi_i q_{s2,i}\right)^2},\ \ INT2_j = 2\int_0^1 \frac{\phi_j^2 H_e(x) dx}{\left(R - \sum_{i=1}^n \phi_i q_{s1,i} + \sum_{i=1}^n \phi_i q_{s2,i}\right)^3} \tag{A3}$$

$$INT3_j = 3\int_0^1 \frac{\phi_j^3 H_e(x) dx}{\left(R - \sum_{i=1}^n \phi_i q_{s1,i} + \sum_{i=1}^n \phi_i q_{s2,i}\right)^4},\ \ INT4_j = 4\int_0^1 \frac{\phi_j^4 H_e(x) dx}{\left(R - \sum_{i=1}^n \phi_i q_{s1,i} + \sum_{i=1}^n \phi_i q_{s2,i}\right)^5}$$

$$INT5_j = \int_0^1 \frac{\phi_j H_e(x) dx}{\left(1 - \sum_{i=1}^n \phi_i q_{s2,i}\right)^2},\ \ INT6_j = 2\int_0^1 \frac{\phi_j^2 H_e(x) dx}{\left(1 - \sum_{i=1}^n \phi_i q_{s2,i}\right)^3},\ \ INT7_j = 3\int_0^1 \frac{\phi_j^3 H_e(x) dx}{\left(1 - \sum_{i=1}^n \phi_i q_{s2,i}\right)^4},$$
$$INT8_j = 4\int_0^1 \frac{\phi_j^4 H_e(x) dx}{\left(1 - \sum_{i=1}^n \phi_i q_{s2,i}\right)^5}$$

Appendix B

In this study, the harmonic balance method is employed to obtain the frequency response curves associated with the present system. This method is used to convert the nonlinear differential equations governing the micro-beam's deflection into the nonlinear algebraic equations governing their corresponding amplitude. According to the main idea of this technique [34], the dynamic counterparts associated with the upper and lower micro-beams are assumed to take the following forms:

$$q_{d1} = \sum_{n=1}^{N}\left\{Q_{c1,n}\cos((2n-1)\Omega t) + Q_{s1,n}\sin((2n-1)\Omega t)\right\} \tag{B1}$$

$$q_{d2} = \sum_{n=1}^{N}\left\{Q_{c2,n}\cos((2n-1)\Omega t) + Q_{s2,n}\sin((2n-1)\Omega t)\right\} \tag{B2}$$

where $Q_{c1,n}$, $Q_{c2,n}$, $Q_{s1,n}$, and $Q_{s2,n}$ ($n = 1, \ldots, N$) denote the coefficients corresponding to each harmonic and also Ω is the excitation frequency. Substituting Eqs. (B1) and (B2) into the reduced equations of motion in Eq. (24) and equating the coefficient of each harmonic, a set of nonlinear algebraic equations relating to the harmonic's coefficients and Ω are obtained. The resulting equations are solved numerically using MATLAB [36] command fsolve with appropriated initial guesses.

References

[1] Ejeian F, Azadi S, Razmjou A, Orooji Y, Kottapalli A, Warkiani ME, et al. Design and applications of MEMS flow sensors: a review. Sensor Actuat A-Phys 2019;295: 483–502. https://doi.org/10.1016/j.sna.2019.06.020.

[2] Younis MI. MEMS linear and nonlinear statics and dynamics. USA: Springer; 2011.

[3] Song J, Lyu M, Kacem N, Liu P, Huang Y, Fan K, et al. Exploiting bifurcation behaviors in parametrically excited mode-localized resonators for mass sensing. J Appl Mech 2022;89(11):111006. https://doi.org/10.1115/1.4055543.

[4] Lee HJ, Park KK, Oralkan Ö, Kupnik M, Khuri-Yakub BT. A multichannel oscillator for a resonant chemical sensor system. IEEE T Ind Electron 2014;61(10):5632–40. https://doi.org/10.1109/TIE.2014.2300031.

[5] Alneamy AM, Ouakad HM. Inertia mass bio-sensors based on snap-through phenomena in electrostatic MEMS shallow arch resonators. Int J Mech Sci 2023; 238:107825. https://doi.org/10.1016/j.ijmecsci.2022.107825.

[6] Manav M, Phani AS, Cretu E. Mode localization and sensitivity in weakly coupled resonators. IEEE Sens J 2018;19(8):2999–3007. https://doi.org/10.1109/JSEN.2018.2889646.

[7] Nikfarjam H, Megdadi M, Okour M, Pourkamali S, Alsaleem F. Theoretical and Experimental investigation of using multi-degree of freedom electrostatically actuated micro-structures in performing classification problems. IEEE Sens J 2023; 23(11):12049–57. https://doi.org/10.1109/JSEN.2023.3265908.

[8] Anderson PW. Absence of diffusion in certain random lattices. Phys Rev 1958;109 (5):1492. https://doi.org/10.1103/PhysRev.109.1492.

[9] Spletzer M, Raman A, Wu AQ, Xu X, Reifenberger R. Ultrasensitive mass sensing using mode localization in coupled microcantilevers. Appl Phys Lett 2006;88(25): 254102. https://doi.org/10.1063/1.2216889.

[10] Pierre C, Dowell E. Localization of vibrations by structural irregularity. J Sound Vib 1987;114(3):549–64. https://doi.org/10.1016/S0022-460X(87)80023-8.

[11] Hajjaj A, Jaber N, Ilyas S, Alfosail F, Younis MI. Linear and nonlinear dynamics of micro and nano-resonators: review of recent advances. Int J Nonlin Mech 2020; 119:103328. https://doi.org/10.1016/j.ijnonlinmec.2019.103328.

[12] Zhao C, Montaseri MH, Wood GS, Pu SH, Seshia AA, Kraft M. A review on coupled MEMS resonators for sensing applications utilizing mode localization. Sensor Actuat A-Phys 2016;249:93–111. https://doi.org/10.1016/j.sna.2016.07.015.

[13] Thiruvenkatanathan P, Seshia A. Mode-localized displacement sensing. J Microelectromech S 2012;21(5):1016–8. https://doi.org/10.1109/JMEMS.2012.2198047.

[14] Leissa AW. On a curve veering aberration. Z ANGEW MATH PHYS 1974;25: 99–111. https://doi.org/10.1007/BF01602113.

[15] Pachkawade V. State-of-the-art in mode-localized MEMS coupled resonant sensors: a comprehensive review. IEEE Sens J 2021;21(7):8751–79. https://doi.org/10.1109/JSEN.2021.3051240.

[16] Pierre C. Mode localization and eigenvalue loci veering phenomena in disordered structures. J Sound Vib 1988;126(3):485–502. https://doi.org/10.1016/0022-460X(88)90226-X.

[17] Thiruvenkatanathan P, Yan J, Woodhouse J, Seshia AA. Enhancing parametric sensitivity in electrically coupled MEMS resonators. J Microelectromech S 2009;18 (5):1077–86. https://doi.org/10.1109/JMEMS.2009.2025999.

[18] Zhao C, Wood GS, Xie J, Chang H, Pu SH, Kraft M. A three degree-of-freedom weakly coupled resonator sensor with enhanced stiffness sensitivity. J Microelectromech S 2015;25(1):38–51. https://doi.org/10.1109/JMEMS.2015.2490204.

[19] Rabenimanana T, Walter V, Kacem N, Le Moal P, Bourbon G, Lardies J. Mass sensor using mode localization in two weakly coupled MEMS cantilevers with different lengths: design and experimental model validation. Sensor Actuat A-Phys 2019; 295:643–52. https://doi.org/10.1016/j.sna.2019.06.004.

[20] Pandit M, Zhao C, Sobreviela G, Du S, Zou X, Seshia A. Utilizing energy localization in weakly coupled nonlinear resonators for sensing applications. J Microelectromech S 2019;28(2):182–8. https://doi.org/10.1109/JMEMS.2019.2894953.

[21] Lyu M, Zhao J, Kacem N, Liu P, Tang B, Xiong Z, et al. Exploiting nonlinearity to enhance the sensitivity of mode-localized mass sensor based on electrostatically coupled MEMS resonators. Int J Nonlin Mech 2020;121:103455. https://doi.org/10.1016/j.ijnonlinmec.2020.103455.

[22] Lochon F, Dufour I, Rebiere D. An alternative solution to improve sensitivity of resonant microcantilever chemical sensors: comparison between using high-order modes and reducing dimensions. Sensor Actuat B-Chem 2005;108(1–2):979–85. https://doi.org/10.1016/j.snb.2004.11.086.

[23] Lyu M, Zhao J, Kacem N, Tang B, Liu P, Song J, et al. Computational investigation of high-order mode localization in electrostatically coupled microbeams with distributed electrodes for high sensitivity mass sensing. Mech Syst Signal PR 2021; 158:107781. https://doi.org/10.1016/j.ymssp.2021.107781.

[24] Zhao J, Song J, Lyu M, Kacem N, Liu P, Huang Y, et al. An asymmetric mode-localized mass sensor based on the electrostatic coupling of different structural modes with distributed electrodes. Nonlinear Dynam 2022;108(1):61–79. https://doi.org/10.1007/s11071-021-07189-2.

[25] COMSOL Multiphysics, Version 6, Burlington MA 01803, 2021 (https://www.comsol.com).

[26] Reddy JN. Theory and analysis of elastic plates and shells. USA: CRC Press; 2006.

[27] Reddy JN. Energy principles and variational methods in applied mechanics. USA: John Wiley & Sons; 2017.

[28] Batra R, Porfiri M, Spinello D. Vibrations of narrow microbeams predeformed by an electric field. J Sound Vib 2008;309(3–5):600–12. https://doi.org/10.1016/j.jsv.2007.07.030.

[29] Chen D, Zhang H, Sun J, Pandit M, Sobreviela G, et al. Ultrasensitive resonant electrometry utilizing micromechanical oscillators. Phys Rev Appl 2020;14(1): 014001. https://doi.org/10.1103/PhysRevApplied.14.014001.

[30] Rao SS. Vibration of continuous systems. USA: John Wiley & Sons; 2019.

[31] Alkaddour M, Ghommem M, Najar F. Nonlinear analysis and effectiveness of weakly coupled microbeams for mass sensing applications. Nonlinear Dynam 2021; 104:383–97. https://doi.org/10.1007/s11071-021-06298-2.

[32] Rezazadeh G, Tahmasebi A, Zubstov M. Application of piezoelectric layers in electrostatic MEM actuators: controlling of pull-in voltage. Microsyst Technol 2006;12:1163–70. https://doi.org/10.1007/s00542-006-0245-5.

[33] Zhao C, Pandit M, Sobreviela G, Mustafazade A, Du S, Zou X, et al. On the noise optimization of resonant MEMS sensors utilizing vibration mode localization. Appl Phys Lett 2018;112(19). https://doi.org/10.1063/1.5025818.

[34] Krack M, Gross J. Harmonic balance for nonlinear vibration problems. Switzerland: Springer; 2019.

[35] Walter V, Bourbon G, Le Moal P, Kacem N, Lardies J. Electrostatic actuation to counterbalance the manufacturing defects in a MEMS mass detection sensor using mode localization. Proc Eng 2016;168:1488–91. https://doi.org/10.1016/j.proeng.2016.11.431.

[36] MATLAB, Version R2016b, Natick MA, 2016 (http://www.mathworks.com).